SUPPLEMENTAL MATERIAL

SUPPLEMENTAL METHODS

Voltage protocols in patch-clamp experiments

K^+ currents were measured in the whole-cell patch-clamp at 37±0.1°C.

Voltage-gated K^+ currents (I_{to}, $I_{K,slow}$ and I_{SS}) were activated using 4.5 s long depolarizing pulses ranging from −40 mV to +60 mV arising from a holding potential of −80 mV and repeated in every 10 s. I_{to} and $I_{K,slow}$ were separated using biexponential fitting (R^2>0.9 in each case) and low-dose 4-aminopyiridne treatment (50 μM), which selectively inhibits $I_{K,slow}$ [2, 14]. $I_{K,slow}$ was present only in mouse but not in rat and rabbit ventricular myocytes. I_{SS} was separated from I_{to} and $I_{K,slow}$ using high-dose (3 mM) 4-aminopyridine treatment. I_{SS} magnitude was measured at the end of the 4.5 s long depolarizing pulse. I_{to} inactivation was assessed following low-dose (50 μM) 4-aminopyridine treatment. Time course of I_{to} recovery from inactivation was studied using a twin-pulse protocol. Two 500 ms long depolarizations to +40 mV were separated by interpulse intervals (with a holding potential of −80 mV) having variable durations. Peak I_{to} amplitude (peak−pedestal at the end of the 500-ms pulse) measured by the second pulse was normalized to that measured by the first pulse, and their ratio (I_2/I_1) was plotted against the interpulse interval.

I_{K1} was measured as Ba^{2+}-sensitive steady-state current at the end of the 500-ms long test pulses between −140 mV and −40 mV in 10 mV steps.

I_{Kr} was activated by 3 s long depolarizing pulses to +40 mV arising from the holding potential of −80 mV. I_{Kr} was assessed as the E-4031-sensitive tail current amplitudes recorded following repolarization to −40 mV.

Drug treatments

The effect of acute treatment with high glucose (30 mM) was assessed following 6 min perfusion in the same cell in self-controlled experiments. Details on drug treatments, doses and supporting references are provided below.

K^+ currents were separated using 4-aminopyridine to selectively inhibit $I_{K,slow}$ in low-dose (50 μM) and both I_{to} and $I_{K,slow}$ in high-dose (3 mM) [2, 14], E-4031 (1 μM) to selectively inhibit I_{Kr} [8, 13], and $BaCl_2$ (300 μM) to inhibit I_{K1} [1, 9].

To examine specific signaling pathways, cell pretreatments with selective inhibitors started 15-30 min before the experiments and the drugs were also added to both the perfusion and the pipette solutions.

To assess the contribution of *O*-GlcNAcylation in K^+ channel regulation during hyperglycemia, the following inhibitors were used: 6-diazo-5-oxo-L-norleucine (DON, 50 μM) to inhibit a broad spectrum of amidotransferases, including the glutamine-fructose-6-phosphate amidotransferase which is the first and rate-limiting enzyme in the hexosamine biosynthetic pathway [5], OSMI-1 (50 μM) to selectively inhibit *O*-GlcNAc transferase [7], and Thiamet-G (Thm-G, 100 nM) to selectively inhibit *O*-GlcNAc*ase* [15].

To assess the contribution of protein kinases in K^+ channel regulation during hyperglycemia, the following inhibitors were used: autocamtide-2-related inhibitory peptide (AIP, 1 μM) to selectively inhibit CaMKII [4], protein kinase inhibitor peptide (PKI, 1 μM) to selectively inhibit PKA [12], and bisindolylmaleimide II (BIM-II, 100 nM) and Go 6976 (100 nM) to selectively inhibit PKC [6, 10]. In the extracellular solution, the cell-permeable myristoylated forms of PKI and AIP were used. As a negative control for PKC inhibitors, bisindolylmaleimide V (BIM-V, 100 nM) was used.

To assess the contribution of ROS in K^+ channel regulation during hyperglycemia, a combination of ROS scavengers was used: reduced glutathione (GSH, 10 mM) [11] and N-acetylcysteine (NAC, 10 mM) [3].

Chemicals were purchased from Sigma-Aldrich (St. Louis, MO, USA), if not specified otherwise. Tetrodotoxin and Go 6976 were from Calbiochem (Burlington, MA, USA), E-4031 was from Tocris (Bristol, UK), and BIM-V was from Santa Cruz Biotechnology (Dallas, TX, USA).

Gene	Protein	I_K	Forward primer (5' to 3')	Reverse primer (5' to 3')
Gapdh	GAPDH	N/A	AACAGCAACTCCCACTCTTC	CCTGTTGCTGTAGCCGTATT
S18	18S rRNA	N/A	AAAGCAGACATCGACCTCAC	GTACTTCCCATCCTTCACATCC
Camk2d	CaMKIIδ	N/A	GTGACACCTGAAGCCAAAGA	CATCATGGAGGCAACAGTAGAG
Camk2g	CaMKIIγ	N/A	AAGCTGGAGCCTACGATTTC	GCGCTTTGCAGGGTTTAT
Anf	ANF	N/A	CAGGCCATATTGGAGCAAATC	GGGCATGACCTCATCTTCTAC
Myh7	β-MHC	N/A	AGATGGCTGGTTTGGATGAG	TTGGCCTTGGTCAGAGTATTG
Kcnd2	K_V4.2	$I_{to,fast}$	CGCCACATCCTCAACTTCTA	CGGTCCTTGTACTCCTCATAAC
Kcnd3	K_V4.3	$I_{to,fast}$	GTGGCCATCATGCCCTATTA	GAAGATCCTGAAGACACGGAAG
Kcnip2	KChIP2	$I_{to,fast}$	TGATAGACTGAACTGGGCTTTC	GTAGGTGTACTTGCCCATCAT
Kcna4	K_V1.4	$I_{to,slow}$	ATCGTGGAGACAGTGTGTATTG	GCCCAGAGTGATGAAGTAAGG
Kcna5	K_V1.5	$I_{K,slow}$	TGAGGATGAGGAGGGAGAAG	CGCAAACCCGAGATGTTTATG
Kcnb1	K_V2.1	$I_{K,slow}$	GGCTTGTATCACGATCCTCTTAG	GCACTTGCTGTGGTGTAGAT
Kcnk2	TREK-1	I_{ss}	CTGTTTGGCTGTGTCCTCTT	CTGCCACGTAGTCTCCAAATC
Kcnk3	TASK-1	I_{ss}	GGACTTTCTTCCAGGCCTATT	GAAGCTGAAGGCCACATACT
Kcnj2	K_{ir}2.1	I_{K1}	GGTACCTGGCAGACATCTTTAC	GAGCAGGGCTATCAACCAAA
Kcnj12	K_{ir}.2.2	I_{K1}	AAGGGCCTAGACCGTATCTT	CTCAAAGTCGTCTGTCTCAAGG
Kcnh2a	hERG1a	I_{Kr}	CCCTCCATCAAGGACAAGTATG	GCATGACACAGATGGAGAAGA
Kcnh2b	hERG1b	I_{Kr}	GCTTACTGCCCTCTACTTCATC	CTTTCCAGGACGGGCATATAG
Kcnq1	K_V7.1	I_{Ks}	CTGGGCTCTGTAGTCTTCATTC	CTCGTTCACCGCATCTTTCT
Kcne1	MinK	I_{Ks}	CCCAATTCCACGACTGTTCT	CAGCACCATGAGGATGTAGAG

Supplemental Table 1. The sequence of specific primers used in qRT-PCR.
Examined genes, encoded proteins and related K^+ currents (if applicable) with the corresponding forward and reverse primers are listed.

	WT + Vehicle		WT + STZ	
	Pre-inj.	4-wk Post-inj.	Pre-inj.	4-wk Post-inj.
N (animals)	7		5	
FS (%)	21.3±2.3	20.4±1.0^{NS}	24.6±3.8	24.0±0.8^{NS}
LVIDd (mm)	3.90±0.23	4.05±0.13^{NS}	3.82±0.15	4.06±0.13^{NS}
LVIDs (mm)	3.11±0.25	3.22±0.10^{NS}	2.90±0.24	3.06±0.08^{NS}
LVPWd (mm)	0.88±0.08	0.82±0.03^{NS}	0.82±0.11	0.71±0.03^{NS}
LVPWs (mm)	1.24±0.11	1.14±0.08^{NS}	1.15±0.12	0.95±0.05^{NS}
IVSd (mm)	0.92±0.06	0.92±0.4^{NS}	0.88±0.08	0.84±0.09^{NS}
IVSs (mm)	1.18±0.06	1.25±0.06^{NS}	1.25±0.10	1.21±0.07^{NS}

Supplemental Table 2. Echocardiography parameters in diabetic mice.

Cardiac contractile function was assessed by M-mode echocardiography before and 4 weeks after low-dose streptozotocin (STZ) injection (for 5 consecutive days) to induce type 1 diabetes mellitus versus vehicle control in wild-type (WT) male mice. Comparisons between pre- and post-injection parameters were made using Student's paired *t* test, *NS* indicates non-significance.

(FS, fractional shortening, calculated as FS=(LVIDd-LVIDs)/LVIDd x 100; LVIDd and LVIDs, left ventricular end-diastolic and end-systolic diameters, respectively; LVPWd and LVPWs, left ventricular posterior wall thicknesses at diastole and at systole, respectively; IVSd and IVSs are intraventricular septal thicknesses at diastole and at systole, respectively.)

	WT + Sham		WT + TAC	
	Pre-op	8-wk Post-op	Pre-op	8-wk Post-op
N (animals)	3		4	
FS (%)	22.4±2.0	22.4±0.8^{NS}	20.5±2.1	11.4±1.2$^{P=0.01}$
LVIDd (mm)	3.86±0.19	4.34±0.33^{NS}	4.02±0.14	4.66±0.12$^{P=0.02}$
LVIDs (mm)	2.99±0.16	3.37±0.29^{NS}	3.20±0.17	4.13±0.14$^{P=0.01}$
Heart weight (mg)	*N/A*	0.24±0.01	*N/A*	0.40±0.03$^{P=0.01}$
Body weight (mg)	*N/A*	31.6±1.5	*N/A*	32.0±2.2^{NS}
HW / BW (%)	*N/A*	0.76±0.07	*N/A*	1.29±0.17$^{P=0.05}$
Cell capacitance (pF)	*N/A*	148.8±1.8	*N/A*	246.2±8.1$^{P<0.001}$

Supplemental Table 3. Echocardiography and morphometic parameters in heart failure mice.
Cardiac contractile function was assessed by M-mode echocardiography before and 8 weeks after transverse aortic constriction (TAC) surgery to induce heart failure (HF) versus sham control in wild-type (WT) male mice. Enlarged left ventricular dimensions and significantly reduced fraction shortening measured in M-mode echocardiography demonstrate ventricular dilation and functional impairment in HF. Increased heart weight, HW/BW and cell capacitance demonstrate significant myocardial hypertrophy in HF. Student's *t* test, paired (echocardiography) or unpaired (morphometry). *NS* indicates non-significance. *N/A* indicates not applicable.
(FS, fractional shortening, calculated as FS=(LVIDd-LVIDs)/LVIDd x 100; LVIDd and LVIDs, left ventricular end-diastolic and end-systolic diameters, respectively; HW/BW, heart weight to body weight ratio.)

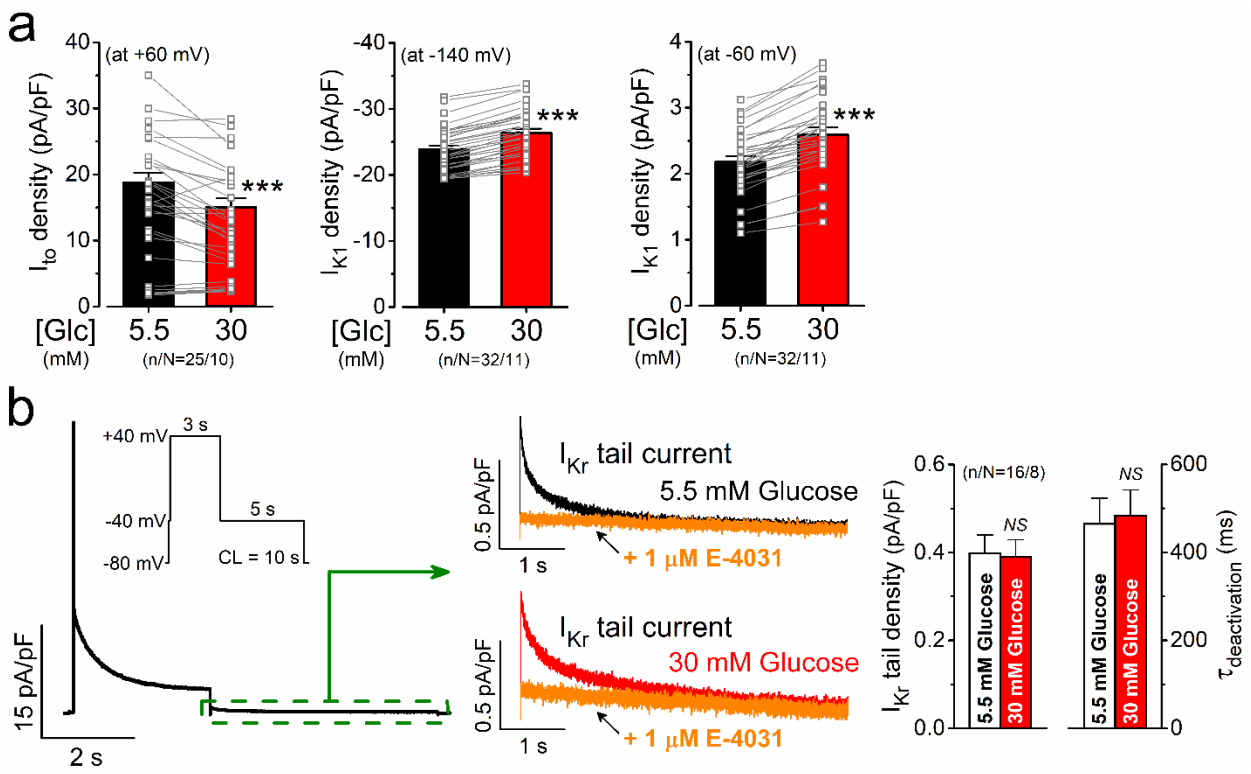

Supplemental Figure 1. Acute hyperglycemia and K^+ currents in mouse ventricular myocytes.
a Acute hyperglycemia (30 mM glucose, 6 min) significantly reduced the transient outward K^+ current (I_{to}) and increased the inward rectifier K^+ current (I_{K1}). Paired data are shown in individual cells. **b** Representative rapid delayed rectifier K^+ current (I_{Kr}) traces and averaged data. I_{Kr} tail current density and deactivation time constant ($\tau_{deactivation}$) were unchanged in acute hyperglycemia.
Student's two-tailed, paired *t*-test; *NS*, non-significant; ***p<0.001.

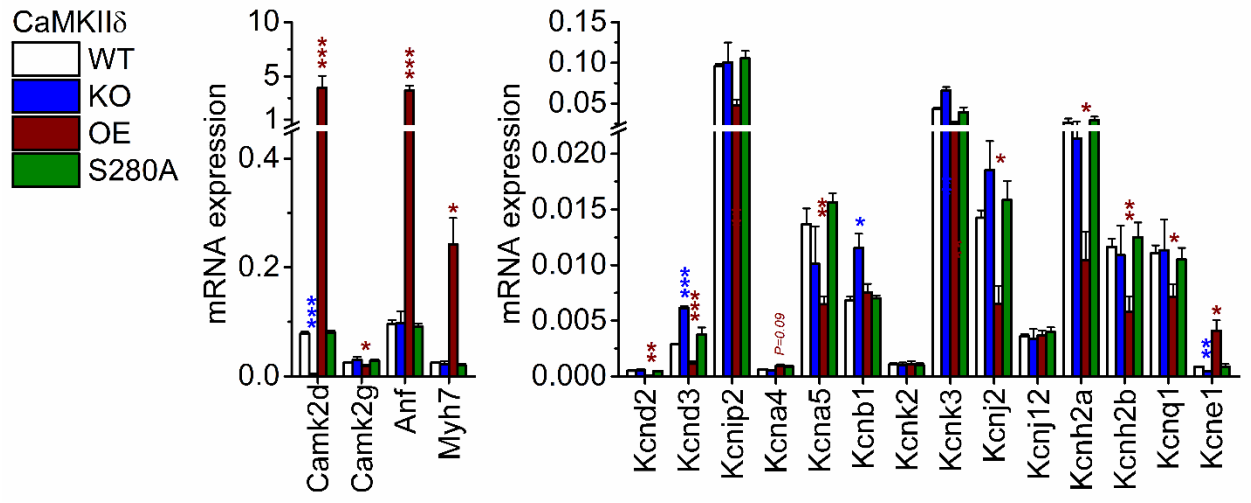

Supplemental Figure 2. mRNA expression of CaMKII and K^+ channel genes.
mRNA expression of Camk2d, Camk2g, hypertrophic markers (Anf, Myh7), and K^+ channel genes assessed by qRT-PCR in WT control, CaMKIIδ-knockout (KO), overexpression (OE) and *O*-GlcNAc-resistant S280A knock-in mouse hearts. ANOVA; *p<0.05, **p<0.01, ***p<0.001.

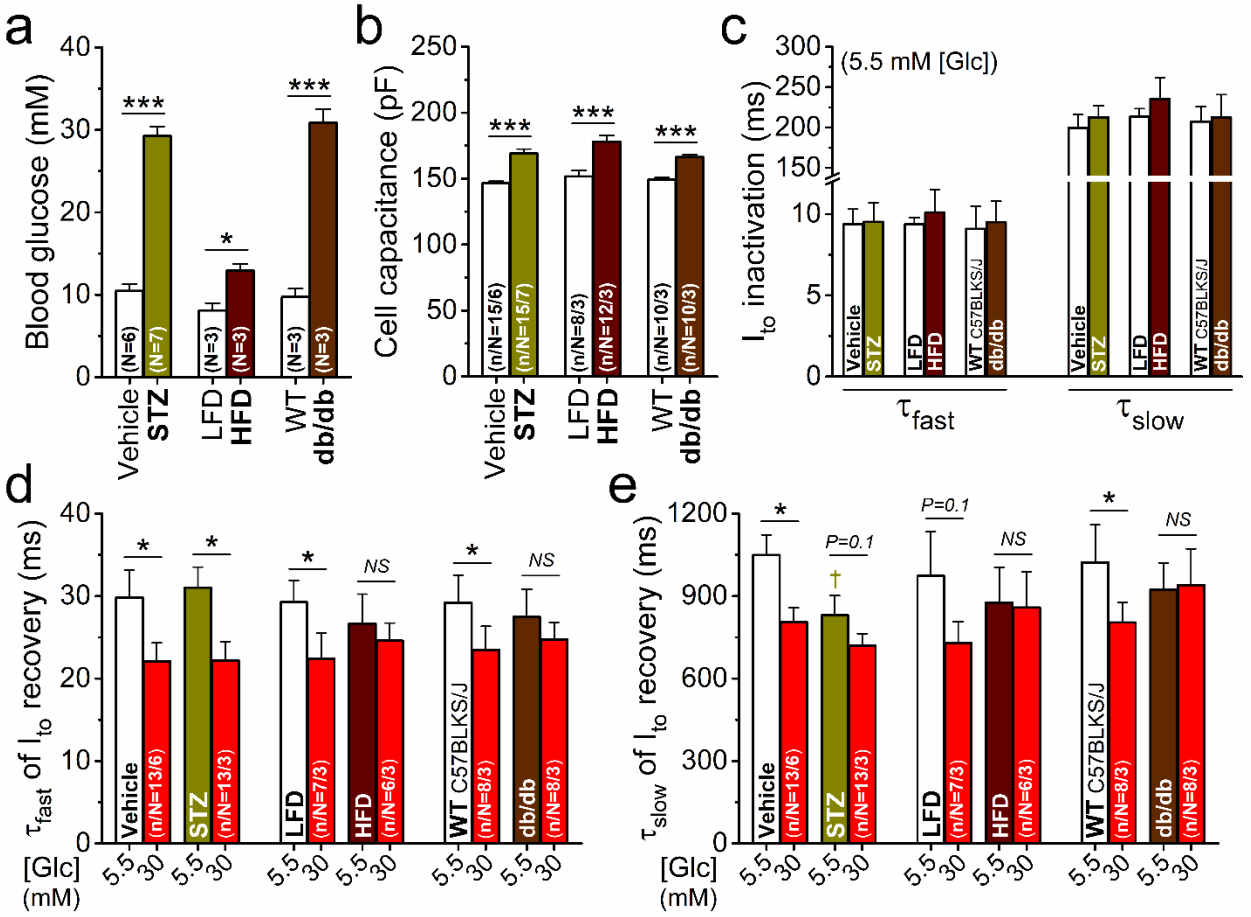

Supplemental Figure 3. Blood glucose levels, cellular hypertrophy, and K^+ current kinetics in diabetes.

a Elevated blood glucose levels in streptozotocin (STZ)-treated type 1 diabetes mellitus (*vs.* vehicle control), in high-fat diet (HFD)-induced type 2 diabetes mellitus (*vs.* low-fat diet, LFD) and in *db*/*db*, a genetic model for type 2 diabetes mellitus (*vs.* wild-type C57BLKS/J). **b** Cardiomyocyte hypertrophy in diabetic mouse models. **c** Inactivation kinetics of the transient outward K^+ current (I_{to}) were unchanged in all diabetic models. **d, e** I_{to} recovery from inactivation kinetics. Hyperglycemia decreased the time constants for both the fast (**d**) and the slow (**e**) components of I_{to} recovery in STZ (and all controls), but not in HFD or *db*/*db*. ANOVA; **p*<0.05, ***p*<0.01, ****p*<0.001 vs. normoglycemia; †*p*<0.05 vs. control.

SUPPLEMENTAL REFERENCES

1. Alagem N, Dvir M, Reuveny E (2001) Mechanism of Ba(2+) block of a mouse inwardly rectifying K+ channel: differential contribution by two discrete residues. J Physiol 534:381-393 doi:10.1111/j.1469-7793.2001.00381.x
2. Brouillette J, Clark RB, Giles WR, Fiset C (2004) Functional properties of K+ currents in adult mouse ventricular myocytes. J Physiol 559:777-798 doi:10.1113/jphysiol.2004.063446
3. Ezerina D, Takano Y, Hanaoka K, Urano Y, Dick TP (2018) N-Acetyl Cysteine Functions as a Fast-Acting Antioxidant by Triggering Intracellular H2S and Sulfane Sulfur Production. Cell Chem Biol 25:447-459 e444 doi:10.1016/j.chembiol.2018.01.011
4. Ishida A, Kameshita I, Okuno S, Kitani T, Fujisawa H (1995) A novel highly specific and potent inhibitor of calmodulin-dependent protein kinase II. Biochem Biophys Res Commun 212:806-812 doi:10.1006/bbrc.1995.2040
5. Marshall S, Bacote V, Traxinger RR (1991) Discovery of a metabolic pathway mediating glucose-induced desensitization of the glucose transport system. Role of hexosamine biosynthesis in the induction of insulin resistance. J Biol Chem 266:4706-4712
6. Martiny-Baron G, Kazanietz MG, Mischak H, Blumberg PM, Kochs G, Hug H, Marme D, Schachtele C (1993) Selective inhibition of protein kinase C isozymes by the indolocarbazole Go 6976. J Biol Chem 268:9194-9197
7. Ortiz-Meoz RF, Jiang J, Lazarus MB, Orman M, Janetzko J, Fan C, Duveau DY, Tan ZW, Thomas CJ, Walker S (2015) A small molecule that inhibits OGT activity in cells. ACS Chem Biol 10:1392-1397 doi:10.1021/acschembio.5b00004
8. Sanguinetti MC, Jurkiewicz NK (1990) Two components of cardiac delayed rectifier K+ current. Differential sensitivity to block by class III antiarrhythmic agents. J Gen Physiol 96:195-215 doi:10.1085/jgp.96.1.195
9. Schram G, Pourrier M, Wang Z, White M, Nattel S (2003) Barium block of Kir2 and human cardiac inward rectifier currents: evidence for subunit-heteromeric contribution to native currents. Cardiovasc Res 59:328-338 doi:10.1016/s0008-6363(03)00366-3
10. Toullec D, Pianetti P, Coste H, Bellevergue P, Grand-Perret T, Ajakane M, Baudet V, Boissin P, Boursier E, Loriolle F, et al. (1991) The bisindolylmaleimide GF 109203X is a potent and selective inhibitor of protein kinase C. J Biol Chem 266:15771-15781
11. Townsend DM, Tew KD, Tapiero H (2003) The importance of glutathione in human disease. Biomed Pharmacother 57:145-155 doi:10.1016/s0753-3322(03)00043-x
12. Walsh DA, Ashby CD, Gonzalez C, Calkins D, Fischer EH (1971) Krebs EG: Purification and characterization of a protein inhibitor of adenosine 3',5'-monophosphate-dependent protein kinases. J Biol Chem 246:1977-1985
13. Wettwer E, Scholtysik G, Schaad A, Himmel H, Ravens U (1991) Effects of the new class III antiarrhythmic drug E-4031 on myocardial contractility and electrophysiological parameters. J Cardiovasc Pharmacol 17:480-487 doi:10.1097/00005344-199103000-00018
14. Xu H, Guo W, Nerbonne JM (1999) Four kinetically distinct depolarization-activated K+ currents in adult mouse ventricular myocytes. J Gen Physiol 113:661-678 doi:10.1085/jgp.113.5.661
15. Yuzwa SA, Macauley MS, Heinonen JE, Shan X, Dennis RJ, He Y, Whitworth GE, Stubbs KA, McEachern EJ, Davies GJ, Vocadlo DJ (2008) A potent mechanism-inspired O-GlcNAcase inhibitor that blocks phosphorylation of tau in vivo. Nat Chem Biol 4:483-490 doi:10.1038/nchembio.96